Frequency-locked, quasiperiodic, and chaotic motions of current-density filaments in a semiconductor device

F.-J. Niedernostheide, C. Brillert, B. Kukuk, and H.-G. Purwins
Institut für Angewandte Physik, Universität Münster, Corrensstraße 2/4, D-48149 Münster, Germany

H.-J. Schulze
Siemens AG, Otto-Hahn-Ring 6, D-81370 München, Germany

(Received 13 June 1996)

Silicon multilayered devices biased with a dc voltage exhibit spontaneous voltage oscillations which are connected with spatial, pendulumlike oscillations of a current-density filament. When driven with a superimposed sinusoidal voltage, the oscillations of the device voltage show frequency locking, quasiperiodicity, and chaos. In order to correlate the global voltage oscillations with the filament motion spatially resolved measurements of the filament dynamics have been performed by using two different techniques: measurements of the recombination radiation with a streak camera and measurements of the potential on the device surface between the electrical contacts with an active potential probe. The experimental results clearly reveal that the various kinds of voltage oscillations are caused by corresponding frequency-locked, quasiperiodic, or chaotic filament motions. [S0163-1829(96)05143-0]

I. INTRODUCTION

In nonlinear dissipative systems, a huge variety of instabilities leading to the appearance of self-sustained oscillations has been investigated both experimentally and theoretically in the last three decades. It has been shown for diverse biological, chemical, and physical systems that the interplay of the internally generated oscillation with an external periodically oscillating driving force can lead to such interesting phenomena as frequency locking, quasiperiodicity and chaos (for a review see, e.g., Ref. 1). The well-known one-dimensional discrete standard circle map turned out to be of fundamental importance for studying such phenomena. It describes the evolution of the phase of a driven oscillating system measured at periodic time intervals which are given by the period of the external driving force. The analysis of the circle map revealed universal scaling laws and behavior[2–5] which made it a generic map for describing dissipative systems with two competing frequencies.

In semiconductors and semiconductor devices, partly excellent quantitative agreement between the predictions of the circle map and experiments have been obtained. In particular, quasiperiodic and chaotic oscillations and transitions between them have been studied in detail, e. g., in ac driven n- (Refs. 6 and 7) and p-type Ge,[8–10] as well as in n-type GaAs.[11,12] Most investigations have been performed by analyzing time series of global quantities, e.g., the device current or voltage. However, in all examples mentioned, spatially nonuniform distributions of local quantities, e.g., the carrier density, current density, or electric field, are known, or at least assumed to cause the oscillation of the global quantity.

Current-density filaments and electric-field domains are two prominent examples of such spatial structures. In many cases, the dynamic behavior of these two structures can be reduced to a few fundamental modes: oscillations of the amplitude, the width, or the center of the structure. Obviously, the appearance of complex spatial structures can be expected when a self-sustained oscillation of the aforementioned kind is forced by an external periodic driver. For driven Gunn diodes mode locking and irregular spatiotemporal behavior of traveling field domains have been predicted in numerical simulations.[13] However, experimental confirmation has yet to be seen. Recently, detailed spatially resolved measurements on the spatiotemporal behavior of the electric field related with the complex dynamics of space-charge domains have been performed in driven p-type ultrapure Ge[14,15] and a set of rate equations within the drift-diffusion approximation has been used to describe the experimentally observed behavior.[26] They gave clear evidence of mode locking and spatially coherent as as well as incoherent variations of the electric field. Periodically and irregularly switching current-density filaments are proposed to explain the phenomena observed in driven n-type GaAs.[12,16,17]

In this paper we investigate the dynamics of a sinusoidally driven rocking current-density filament, i.e., a filament performing spatial, pendulumlike periodic oscillations, thus representing one of the aforementioned basic oscillation modes. Section II presents details concerning the investigated p^+-n^+-p-n^- samples, and briefly describes the properties of the dc-biased samples. The global response of the system on sinusoidal ac excitation is studied in Sec. III by analyzing the time series of the device voltage as a function of the amplitude and frequency of the ac drive. The experiments presented show that the interaction of the external drive with the self-generated oscillation leads to universal behavior and bifurcation routes as predicted by the circle map. In Sec. IV we focus on the spatiotemporal dynamics of the driven rocking filament. Spatially resolved measurements of the electroluminescence radiation and the potential reveal that the observed frequency-locked, quasiperiodic, and chaotic oscillations of the device voltage can be correlated to corresponding rocking motions of the filament. Some conclusions are presented in Sec. V.

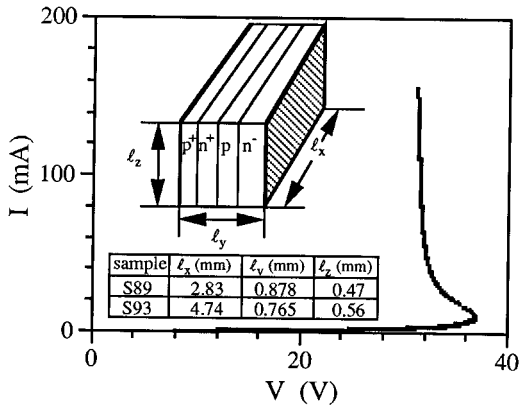

FIG. 1. Current-voltage characteristic $I(V)$ of sample S89 at room temperature. The inset shows a schematic sketch of the sample and geometric dimensions of the two samples the results presented in this work refer to.

II. EXPERIMENTAL DETAILS

The p^+-n^+-p-n^- samples used for the measurements were prepared from a lightly doped n-type (111) silicon wafer with a resistivity of 500 Ω cm. The p-doped layer was fabricated by an aluminium vacuum predeposition with a subsequent drive-in step, the n^+ layer by a phosphorus diffusion. The top p^+ layer was produced by boron implantation. At the bottom of the high-resistivity substrate an additional n^+ layer was formed by phosphorus implantation to provide a nonblocking electrical contact. Finally, aluminium layers were evaporated on both wafer sides. After cutting the wafer into rectangular samples the four fractured surfaces were polished to reduce surface damage. The sample characteristics are described in detail in Ref. 18.

The measurements are carried out with the samples clamped between two aluminium jaws the temperature of which is fixed with an accuracy of 0.1 K. The samples are connected to an amplifier via a load resistor R_0. The output voltage $V_s(t)$ of the amplifier is given by

$$V_s(t)=V_{s0}+V_d\sin(2\pi f_d t), \tag{1}$$

where V_{s0} is the dc part of the applied voltage, V_d is the drive amplitude, and f_d is the drive frequency. In order to minimize thermal heating of the samples the voltage is switched on for relatively short periods of 200–600 ms followed by a waiting period of the order of 100 s.

First, we briefly discuss the case $V_d=0$, i. e., a pure dc voltage V_{s0} is applied to the p^+-n^+-p-n^- diodes with the p^+ layer positively biased with respect to the n^- substrate. The n^+-p junction is reverse biased, and limits the total current flowing through the device. For sufficiently large device voltages ($\approx$ 40 V) the electric field in the space-charge region of this junction becomes large enough to effect carrier multiplication by impact ionization. The generated electron-hole pairs are separated in the high-field zone; the electrons move toward the p^+ anode, the holes toward the n^- cathode. There they may cause an additional carrier injection leading to a positive feedback and an increase of the device current. Figure 1 shows a typical current-voltage characteristic of the device. The inset of Fig. 1 illustrates the sample geometry with the dimensions of the two samples belonging to the experiments presented in this paper.

It has been shown in a previous work that the autocatalytic current increase is accompanied by the evolution of a static current-density filament that is stabilized by two competing processes:[18,19] On the one side the autocatalytic carrier multiplication stimulates the formation of the filament, while on the other side the increasing current density causes an increase of the voltage V_p across the p-n^- junction, which counteracts the current increase. Due to the large carrier lifetime of about 100 μs in the n^- layer, a spreading of the current-density filament takes place in this layer causing a corresponding broadly peaked distribution of the voltage V_p, so that the inhibiting mechanism also becomes effective far away from the filament center and leads to the stabilization of the filament.

When a critical device current is exceeded, spontaneous oscillations of the device voltage with a frequency of the order of several kHz appear. It turned out that these oscillations are accompanied by a pendulumlike oscillation of the whole filament around a fixed position in space.[18,19] Again the competition between the activating and inhibiting process can explain the observed oscillation, making use of the fact that the lateral spreading of the activating mechanism is faster than that of the inhibiting process[19,20]. The amplitudes of the oscillation of the device voltage and current are very small, typically in the range of few tenths of a percent up to a few percents of the dc parts. They are probably caused by small fluctuations in the width and amplitude of the current-density filament. Increasing the dc bias, we observe a continuous increase of the spatial oscillation followed by a period-doubling sequence and an irregular filament motion[21]. This behavior has been found in more than 40 samples cut from two different wafers.

III. NONLOCAL ANALYSIS

As mentioned above, the main aim of our work is to investigate the spatiotemporal dynamics of a driven rocking current-density filament. Therefore, for all results presented in this paper the dc bias has been adjusted such that the rocking motion of the filament is simply periodic. In this section we analyze the global system response on an external drive by studying the dependence of the device voltage on the drive frequency f_d and the drive amplitude V_d. In Sec. IV we relate the global response behavior to the local filament dynamics. As a result we are able to supply a complete classification of the spatiotemporal behavior of a driven rocking filament in the f_d-V_d control parameter space.

When the drive amplitude is relatively small, the temporal behavior of the device voltage is either periodic or quasiperiodic. Examples for frequency-locked oscillations are shown in Figs. 2(a) and 2(b). In the first two columns, the time series of the applied ac drive voltage $\tilde{V}_d(t)=V_d\sin(2\pi f_d t)$ are compared with the ac part $\tilde{V}(t)$ of the resulting voltage oscillation $V(t)=V+\tilde{V}(t)$, where V is the mean time value of $V(t)$. The third column of Fig. 2 shows the Poincaré maps, constructed by strobing the device voltage $V(t)$ at the zero passages of the ac drive with a positive slope and plotting the $(n+1)$th vs the nth strobed value. The last column contains the power spectra of $\tilde{V}(t)$.

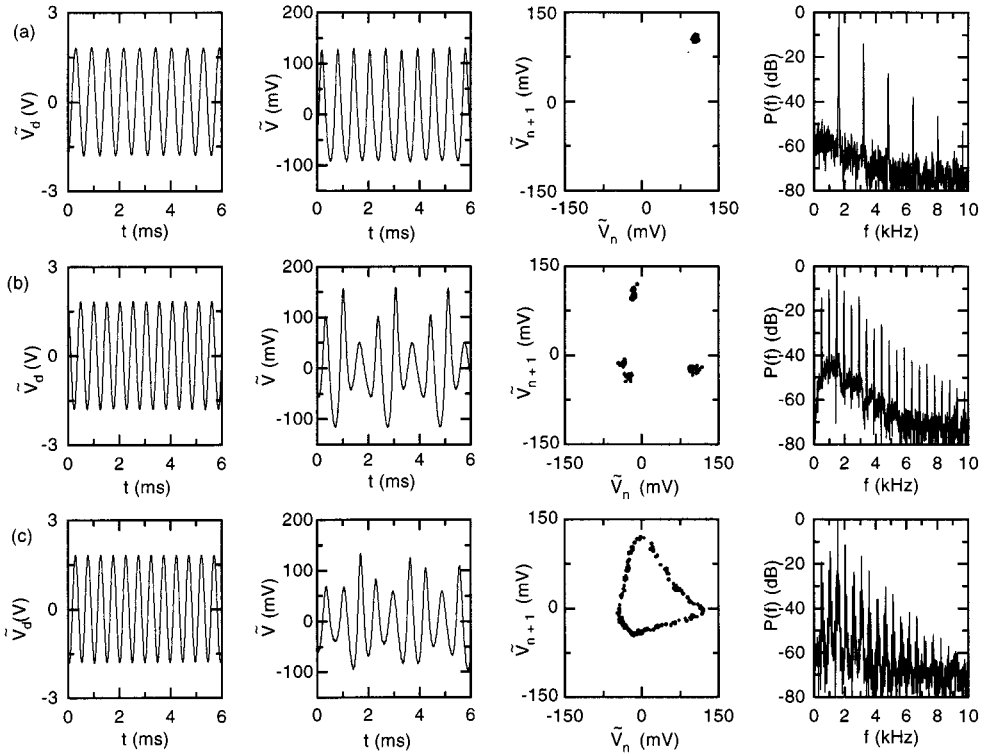

FIG. 2. Time series of the ac drive $\tilde{V}_d(t)$ and the ac part $\tilde{V}(t)$ of the device voltage, Poincaré map constructed from $\tilde{V}(t)$ at a fixed phase of $\tilde{V}_d(t)$, and power spectrum $P(f)$ of $\tilde{V}(t)$ for different values of the drive frequency: $f_d = 1606$ Hz (a), 1953 Hz (b), and 2032 Hz (c). Other parameters are $V_{s0} = 173.7$ V, $V_d = 1.82$ V, $R_0 = 1.01$ kΩ, $T = 287.2$ K, and $f_0 = 1523$ Hz for sample S93.

The data shown in Fig. 2(a) have been taken at a drive ratio $f_0/f_d = 0.95$. The fundamental oscillation frequency for the fixed dc bias $V_{s0} = 173.7$ V is $f_0 = 1523$ Hz. Obviously, the voltage oscillation is frequency locked to the external drive with a 1:1 locking. This is confirmed by the power spectrum in which only the drive frequency (main peak) and its harmonics appear and by the Poincaré map containing only a single point. Figure 2(b) shows an example of a frequency-locked oscillation with a 3:4 locking at a drive ratio $f_0/f_d = 0.78$. In the time series $\tilde{V}(t)$ an amplitude modulation is clearly discernible. The power spectrum reveals a series of equidistant peaks. The distance between two successive peaks is $1/4f_d$. As expected, for a 3:4 locking there are two subharmonics in the spectrum according to the general rule that the number of subharmonics is equal to $P-1$, where P denotes the nominator of the frequency-locked oscillation with a P/Q locking. The number of points appearing in the Poincaré map is equal to the denominator of a P/Q locking in agreement with the four points of the map shown in Fig. 2(b). The oscillation shown in Fig. 2(c) belongs to a drive ratio $f_0/f_d = 0.7495$ that leads to a quasiperiodic behavior. The appertaining power spectrum clearly reveals peaks at the frequency f_0, the fundamental oscillation frequency of the self-sustained oscillation, and at the the drive frequency f_d. Many peaks at frequencies $f = nf_0 + mf_d$ also appear, where n and m are whole numbers. A further indication for the quasiperiodic behavior is given by the Poincaré map which is forming an approximately closed curve, giving evidence of a dense covering of the toroidal attractor.

In Fig. 3 the result of a systematic variation of the drive frequency f_d ($\Delta f_d = 60$ Hz) at fixed drive amplitude is shown. The locking ratio has been experimentally detected by evaluating the local extrema of $\tilde{V}(t)$ and $\tilde{V}_d(t)$ and the power spectrum of $\tilde{V}(t)$. The plateaus in Fig. 3 indicate the frequency intervals in which frequency locking of the voltage oscillation to the external drive with a P/Q locking appears. As predicted by the circle map, the locked regions order in a way that regions with frequency ratios $(P+P')/(Q+Q')$ fall between locked regions with P/Q and P'/Q'. The widths of the latter intervals are always larger than those of the locked intervals in between.

For larger drive amplitudes V_d, the widths of the locking intervals increase and frequency-locking behavior in the f_d-V_d control parameter space is described by a set of Arnold tongues, as shown in Fig. 4. This diagram has been obtained

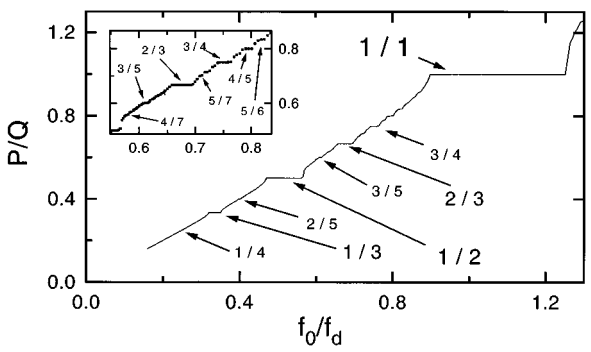

FIG. 3. Locking ratio P/Q as function of the frequency ratio f_0/f_d. Parameters are $V_{s0} = 49.5$ V, $V_d = 352$ mV, $R_0 = 510$ Ω, $T = 314.8$ K, and $f_0 = 4717$ Hz, for sample S89.

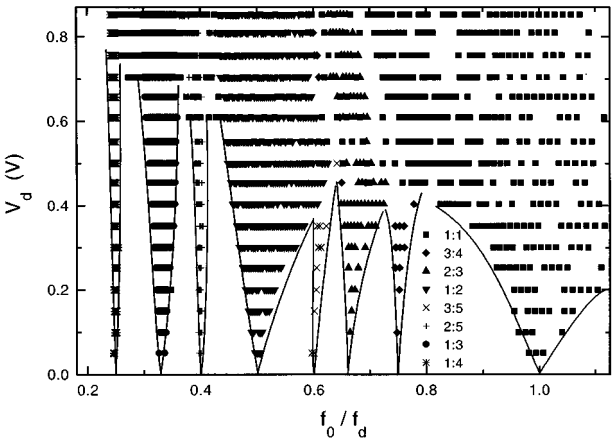

FIG. 4. Arnold tongues in the f_d-V_d control parameter space. Low-order locking ratios are marked by different symbols. The solid lines have been added to guide the eye. Parameters are V_{s0} = 49.2 V, R_0 = 510 kΩ, T = 314.8 K, and f_0 = 4580 Hz for sample S89.

by varying the drive frequency and the drive amplitude in steps of 60 Hz and 50 mV, respectively. For sufficiently large amplitudes the tongues may overlap, indicating a critical line, above which chaotic oscillations may appear in agreement with predictions of the circle map. An example for a chaotic oscillation is shown in Fig. 5(c). In addition to the time series $\tilde{V}(t)$, the projection onto the $\tilde{V}(t+100\ \mu s)$-$\tilde{V}(t)$ phase space, the return map constructed by plotting the $(n+1)$th vs the nth minimum of $\tilde{V}(t)$, and the power spectrum are shown. The large broadband noise in the spectrum and the shape of the projection on the phase space indicate chaotic behavior. The return map is strongly reminiscent of the one-dimensional quadratic map,[22] and gives further evidence that even though the device is spatially extended the dynamics can be reduced to a few degrees of freedom. Note that the chaotic time series presented in Fig. 5(c) is part of a bifurcation sequence observed in the 1:1 Arnold tongue for a large drive amplitude. Starting near the left boundary of the tongue and decreasing the drive frequency, i.e., increasing the ration f_0/f_d we observe a period-doubling cascade, and finally a transition to chaotic behavior. The period-2 and -4 oscillations of this sequence are additionally shown in Figs. 5(a) and 5(b). Similar period-doubling routes have been found in other Arnold tongues for sufficiently large drive amplitudes.

IV. SPATIOTEMPORAL BEHAVIOR

The spatiotemporal behavior of the driven current-density filament has been characterized by applying two different measurement techniques. A streak camera (Hamamatsu C1587) with an infrared sensitive S1 photocathode has been used to image the electroluminescence radiation emitted from one of the polished l_x-l_y surfaces of the sample (Fig. 1). Since the radiation is most effective near the p-n junctions, a small stripe parallel to the anode and comprising the p^+-n^+-p structure of the sample was focused on the photocathode of the streak camera. The weak intensity of the electroluminescence in Si requires that some hundreds of single shots are summed up. Thus this technique is limited to periodic

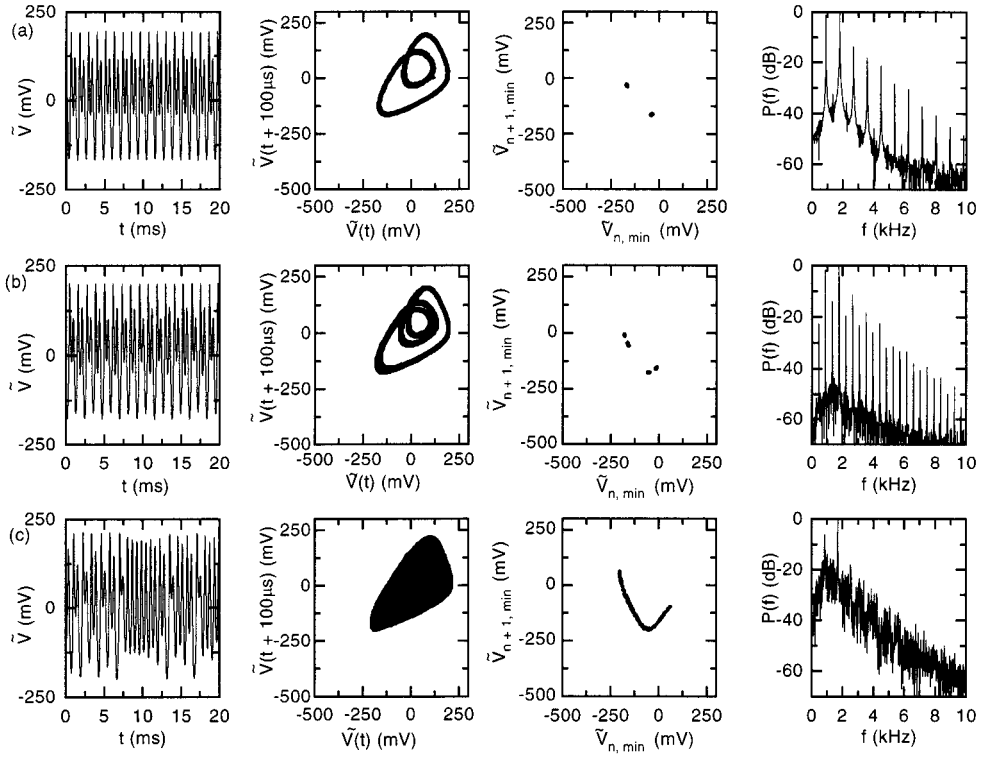

FIG. 5. Period-doubling cascade and chaotic oscillations in the 1:1 Arnold tongue: Time series $\tilde{V}(t)$, projection of the phase space onto the $\tilde{V}(t+100\ \mu s)$-$\tilde{V}(t)$ plane, return map, and power spectrum $P(f)$ for f_d = 1786 Hz (a), 1766 Hz (b), and 1688 Hz (c). Other parameters are V_{s0} = 169.2 V, V_d = 7.10 V, R_0 = 1.01 kΩ, T = 288 K, and f_0 = 1514 Hz for sample S93.

oscillations. In the case of nonperiodic oscillations, measurements with a potential probe (Wentworth, Picoprobe 18B) have been carried out to get information about the filament motion. The low input capacity of the probe of about 0.02 pF leads together with the contact resistance to a time resolution of about 1 μs. The probe is controlled by a micropositioning system so that the potential on the l_x-l_y surface (Fig. 1) between the two aluminium electrodes can be measured with a spatial resolution of about 1 μm.

A. Frequency-locked motions

Figure 6(a) shows a streak camera record for a 2:3 locking of the voltage oscillation to the external drive. The bright regions correspond to regions of high luminescence activity and indicate the current-density filament. The white vertical line marks the left boundary of the sample. Obviously, the filament performs a well-defined oscillation around a certain position with a relatively small spatial amplitude of the order of 100 μm. From the streak camera record a time series of the position $x_c(t)$ of the filament center was constructed [Fig. 6(b)]. This time trace reveals an amplitude and phase modulation in that one period of the voltage oscillation contains two filament elongations of different amplitudes and durations. The time interval of the first elongation, $\Delta t_1 = (0.80 \pm 0.05)$ ms, is larger than that for the second one, $\Delta t_2 = (0.62 \pm 0.05)$ ms, while its spatial amplitude is smaller. A comparison of $x_c(t)$ with the voltage oscillation $\tilde{V}(t)$ [Fig. 6(c)] reveals that both signals are strongly correlated. Within experimental error the local maxima of $\tilde{V}(t)$ coincide with the local minima of $x_c(t)$, i.e., with the maximum filament elongations to the left [Fig. 6(a)]. The same is valid for the local maxima of $x_c(t)$ and the minima of $\tilde{V}(t)$. This asymmetry is due to the fact that the filament oscillates close to the left sample boundary. At the turning point near the boundary, the filament experiences a compression, leading to a decrease of the total current and, accordingly, to an increase of the device voltage. At the other turning point, the filament is stretched and, by this, it is able to carry a slightly larger current. Therefore, the sample voltage decreases. Note that the voltage and current oscillations are only of the order of 0.1–0.5 % of the dc parts. It is obvious from these streak camera measurements that frequency locking is achieved by changes of the amplitude of the rocking motion as well as by variations of the velocity of the filament, the latter is manifested in particular in the fact that the time interval Δt_1 for the smaller elongation is larger than the time interval Δt_2 for the larger elongation.

Potential measurements on the sample surface between the electrodes confirm the strong correlation between the voltage oscillations and the filament motion. An example of spatially dependent potential oscillations for a 1:2 locking of the voltage oscillations with respect to the ac drive is given in Fig. 7(a). The six time series have been taken at six different, equally spaced positions parallel to the anode. The distance from the anode was 109 μm, i.e., the measurements have been performed in the n^- layer close to the p-n^- junction. The continuous decrease of the dc part of the measured potential oscillations from the boundary ($x = 0$) to the interior of the sample [Fig. 7(a)] clearly indicates that the filament is located near the boundary. Therefore, the measurements have been restricted to x coordinates in the interval (0,1.1 mm), while the total length l_x of the sample is 4.74 mm. The amplitudes of the ac parts of the potential oscillations near the turning points [uppermost and lowest curve in Fig. 7(a)] are larger than those in between, as expected for a

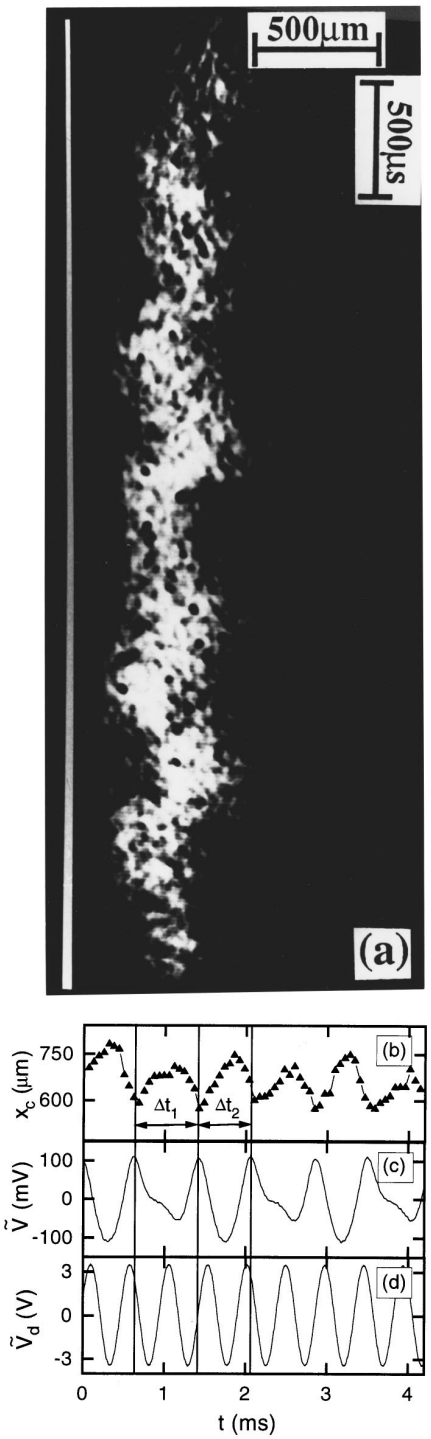

FIG. 6. Motion of a current-density filament for a 2:3 locking of the voltage oscillation to the added ac drive: (a) streak camera record, the vertical white line marks the left sample boundary; (b) time series of the filament center $x_c(t)$ reconstructed from (a), (c) sample voltage $\tilde{V}(t)$, and (d) ac drive voltage $\tilde{V}_d(t)$. Parameters are $V_{s0} = 168.4$ V, $V_d = 3.48$ V, $f_d = 2082$ Hz, $R_0 = 1.01$ kΩ, $T = 288.2$ K, and $f_0 = 1477$ Hz for sample S93.

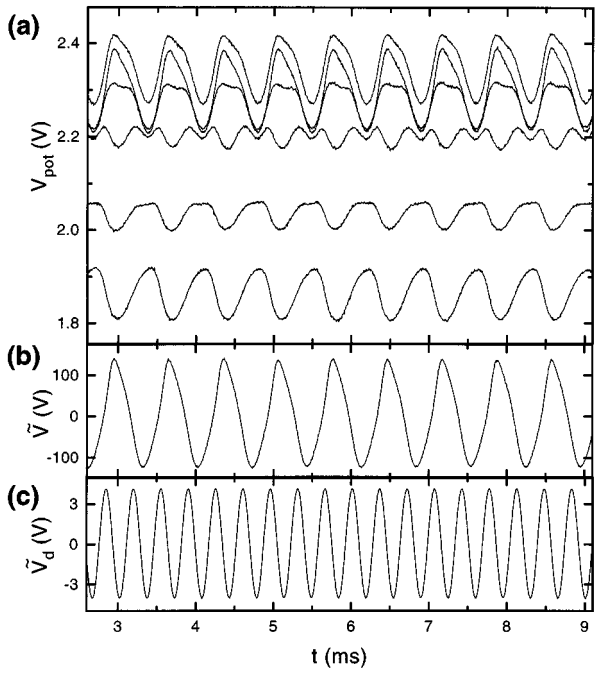

FIG. 7. Local potential $V_{pot}(x,t)$ (a) measured at equally spaced positions on a line parallel to the electric contacts for a 1:2 locking of the sample voltage $\tilde{V}(t)$ (b) with respect to the added ac drive voltage $\tilde{V}_d(t)$ (c). The time series shown in (a) have been recorded at $x = 205$, 380, 556, 730, 904, and 1080 μm (from top to bottom). Parameters are $V_{s0} = 163.4$ V, $V_d = 4.10$ V, $f_d = 2841$ Hz, $R_0 = 1.01$ kΩ, $T = 294.8$ K, and $f_0 = 2330$ Hz for sample S93.

rocking filament motion. A comparison of the spatially dependent potential oscillations with the sample voltage oscillation $\tilde{V}(t)$ [Fig. 7(b)] reveals that the uppermost curve and $\tilde{V}(t)$ are in phase, while the lowest curve and $\tilde{V}(t)$ are in antiphase. Characteristic features of $\tilde{V}(t)$ concerning its shape, however, appear in both potential curves. At x coordinates between the filament turning points, the shapes of the curves are continuously deformed so that the phase differences of the potential oscillations at the turning points can be compensated for. Both streak camera measurements (not shown here), and potential measurements reveal that the filament is oscillating around the position $x = 730$ μm. However, the potential distribution lateral to the main current flow is more extended than the light density distribution in agreement with former measurements of standing and traveling current-density filaments.[18,23] The period of the potential oscillation $V_{pot}(x,t)$ is at all measured x coordinates equal to that of the sample voltage oscillation $\tilde{V}(t)$, the period of which in turn is twice the period of the ac drive $\tilde{V}_d(t)$ indicating the 1:2 locking behavior of the filament motion. Similar correlations between the local filament motion and the global voltage oscillation have been obtained for other locking ratios.

B. Quasiperiodic and chaotic motions

For nonperiodic voltage oscillations the measurement of the electrolumuinescence radiation fails, as the signal-to-noise ratio cannot be improved by adding up several single shots, and the light intensity is too weak for an analysis of a single shot. Therefore, for nonperiodic oscillations we are restricted to measurements with the potential probe.

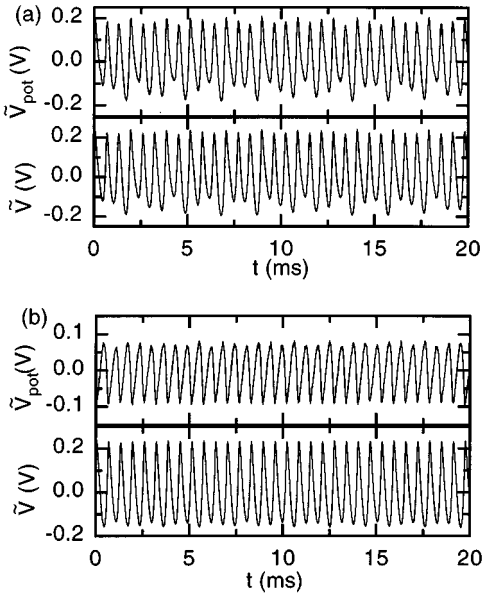

FIG. 8. ac part $\tilde{V}_{pot}(x,t)$ of the local potential and ac part $\tilde{V}(t)$ of the device voltage for a quasiperiodic filament oscillation. $\tilde{V}_{pot}(x,t)$ was measured near the two turning points of the oscillating filament at $x = 156$ (a) and 903 μm (b) in a distance of 210 μm from the anode contact. Parameters are $V_{s0} = 47.09$ V, $f_d = 2.57$ kHz, $f_0 = 1.60$ kHz, $R_0 = 100$ Ω, $T = 303.3$ K, and $V_d = 336$ (a), and 85 mV (b) for sample S93.

Figure 8 shows the time traces of the local potential measured at $x = 156$ μm, close to the left sample boundary and in the interior of the sample at $x = 903$ μm for a drive ratio $f_0/f_d \approx 1602$ Hz/2570 Hz leading to a quasiperiodic oscillation of the sample voltage $\tilde{V}(t)$. The chosen positions for the local potential measurements roughly correspond to the extreme elongations of the oscillating filament. Similar to the periodic, frequency-locked oscillations, the time trace of the potential measured near the sample boundary and that of the sample voltage $\tilde{V}(t)$ are in phase [Fig. 8(a)], while the potential near the interior turning point and $\tilde{V}(t)$ oscillate in antiphase [Fig. 8(b)]. Along the x direction between the turning points the shapes of the potential curve change continuously, enabling the compensation of the phase shifts. For both the local and the global voltage signals the Poincaré maps (not shown here) constructed from the time series result in circlelike curves, indicating a toruslike attractor. Together with the results for frequency-locked filament motions, these results give strong evidence of an approximately pure quasiperiodically rocking filament oscillation. Other oscillation modes, in particular variations in the amplitude and the width of the filament, are also present, but the amplitudes of these oscillations are at least one order of magnitude smaller than that of the rocking motion.

In Fig. 9 the ac part $\tilde{V}_{pot}$ of the local potential measured near the turning point of the rocking filament close to the sample boundary and that of the ac part $\tilde{V}$ of the device voltage are compared for a relatively large drive amplitude. As in the case of periodic and quasiperiodic filament oscillations, the local and global voltage oscillations are in phase.

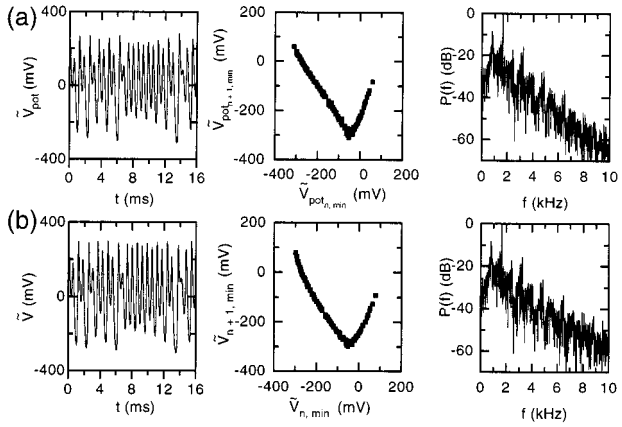

FIG. 9. Time series, return map, and power spectrum of the ac part $\tilde{V}_{\mathrm{pot}}(x,t)$ of the local potential (a) and of the ac part $\tilde{V}(t)$ of the device voltage (b) in the case of a chaotic filament oscillation. $\tilde{V}_{\mathrm{pot}}(x,t)$ was measured at $x = 156$ μm in a distance of 210 μm from the anode contact. Parameters are $V_{s0} = 47.07$ V, $V_d = 805$ mV, $f_d = 1.615$ kHz, $R_0 = 100\ \Omega$, $T = 303.3$ K, and $f_0 = 1.59$ kHz for sample S93.

Chaos is indicated by the shape of the return maps, that have been constructed by using successive local minima of the time series, as well as by the increasing broadband noise in the associated power spectra, in that only the fundamental frequency, the first subharmonic and their harmonics are clearly visible, while other discrete frequencies are less significant. Potential measurements at other x coordinates, which the oscillating filament moves along, reveal comparable correlations between the measured local potential and the global chaotic time series $\tilde{V}(t)$ of the device voltage. However, the phase shift between the local and the global voltage signals is kept, and changes again from 0° at the turning point of the filament oscillation near the sample boundary, to 180° at the other turning point. From these results we may conclude that the chaotic voltage oscillation is correlated with a temporally chaotic but spatially coherent rocking filament motion.

V. CONCLUDING REMARKS AND SUMMARY

The motion of ac driven rocking current-density filaments has been studied by analyzing the temporal evolution of the electroluminescence distribution and the local potential. For medium-sized drive amplitudes and a rational ratio of the self-sustained frequency to the drive frequency, we observe frequency-locked oscillations of the global sample voltage to the external drive that could be clearly attributed to a frequency-locked oscillation of the rocking filament. The spatially and temporally resolved measurements reveal that the filament motion adapts to the external drive by changing the amplitude as well as the duration of the fundamental oscillations. In contrast to self-sustained oscillations, where an increase of the dc bias leads to a monotonic increase of both the spatial amplitude and the period of the oscillation, the ac driven rocking filament may adjust its motion to the external drive by simultaneously lowering the amplitude and increasing the duration of the single oscillation, or vice versa, or even by a combination of both, as has been illustrated for the case of a 2:3 locked filament motion.

For irrational drive ratios the potential on a line parallel to the electric contacts is oscillating quasiperiodically. The observed phase shift of the potential oscillation with respect to the likewise quasiperiodically oscillating sample voltage and its specific variation in space gives, in conjunction with the results for periodic oscillations, strong evidence of a quasiperiodic motion of a rocking filament. Note that quasiperiodic filament motions due to the interaction of two internal oscillation modes of a filament are also conceivable, as has been shown in numerical simulations for the case of interacting width and rocking oscillations of filamentary structures in Refs. 24 and 25. However, an experimental confirmation of such quasiperiodic behavior has yet to be seen.

The systematic variation of the drive amplitude V_d and frequency f_d revealed that the frequency-locked states order in the form of Arnold tongues in V_d-f_d parameter space. It turned out that the tongues may overlap when the drive amplitude is sufficiently large. In this regime period-doubling routes and chaotic filament motions have been observed, in qualitative agreement with predictions of the circle map. We remark that even in the case of chaotic oscillations, the filament dynamic is essentially low dimensional and spatially coherent, indicating the dominance of the rocking mode.

ACKNOWLEDGMENTS

This work was supported in part by the *Deutsche Forschungsgemeinschaft*.

[1] J. A. Glazier and A. Libchaber, IEEE Trans. Circuits Syst. **55**, 790 (1988).
[2] M. J. Feigenbaum, L. P. Kadanoff, and S. J. Shenker, Physica **5D**, 370 (1982).
[3] S. J. Shenkder, Physica **5D**, 405 (1982).
[4] M. H. Jensen, P. Bak, and T. Bohr, Phys. Rev. B **30**, 1960 (1984).
[5] T. Bohr, P. Bak, and M. H. Jensen, Phys. Rev. B **30**, 1970 (1984).
[6] G. A. Held and C. Jeffries, Phys. Rev. Lett. **56**, 1183 (1986).
[7] Y. Kim, Phys. Rev. A **39**, 4801 (1989).
[8] E. G. Gwinn and R. M. Westervelt, Phys. Rev. Lett. **57**, 1060 (1986); **59**, 247(E) (1987).
[9] E. G. Gwinn and R. M. Westervelt, Phys. Rev. Lett. **59**, 157 (1987).
[10] G. Heinz, R. Richter, A. Kittel, G. Flätgen, J. Peinke, and J. Parisi, Phys. Rev. B **48**, 12 603 (1993).
[11] K. Aoki, K. Yamamoto, and N. Mugibayashi, J. Phys. Soc. Jpn. **26**, 26 (1988).
[12] J. Spangler and W. Prettl, Phys. Scr. **T55**, 25 (1994).
[13] E. Mosekilde, R. Feldberg, C. Knudsen, and M. Hindsholm, Phys. Rev. B **41**, 2298 (1990).
[14] A. M. Kahn, D. J. Mar, and R. M. Westervelt, Phys. Rev. Lett. **68**, 369 (1992).

[15] A. M. Kahn, D. J. Mar, and R. M. Westervelt, Phys. Rev. B **46**, 7469 (1992).
[16] K. Aoki and N. Mugibayashi, Appl. Phys. A **48**, 161 (1989).
[17] K. Aoki, in *Negative Differential Resistance and Instabilities in 2-D Semiconductors*, Vol. 307 of *NATO Advanced Study Institute Series B: Physics*, edited by N. Balkan, B. K. Ridley, and A. J. Vickers (Plenum, New York, 1993), pp. 393–407.
[18] F.-J. Niedernostheide, A. Arps, R. Dohmen, H. Willebrand, and H.-G. Purwins, Phys. Status Solidi B **172**, 249 (1992).
[19] F.-J. Niedernostheide, B. S. Kerner, and H.-G. Purwins, Phys. Rev. B **46**, 7559 (1992).
[20] F.-J. Niedernostheide, M. Ardes, M. Or-Guil, and H.-G. Purwins, Phys. Rev. B **49**, 7370 (1994).
[21] F.-J. Niedernostheide, M. Kreimer, H.-J. Schulze, and H.-G. Purwins, Phys. Lett. A **180**, 113 (1993).
[22] M. J. Feigenbaum, J. Stat. Phys. **19**, 25 (1978).
[23] F.-J. Niedernostheide, M. Kreimer, B. Kukuk, H.-J. Schulze, and H.-G. Purwins, Phys. Lett. A **191**, 285 (1994).
[24] F.-J. Niedernostheide, R. Dohmen, H. Willebrand, B. S. Kerner, and H.-G. Purwins, Physica D **69**, 425 (1993).
[25] M. Suzuki, T. Ohta, M. Mimura, and H. Sakaguchi, Phys. Rev. E **52**, 3645 (1995).
[26] M. J. Bergmann, S. W. Teitsworth, L. L. Bonilla, and I. R. Cantalapiedra, Phys. Rev. B **53**, 1327 (1996).